ARMY RESEARCH LABORATORY

An Experimental Approach to Determine the Flight Dynamics of NASA's Mars Science Lab Capsule

by Doug Petrick, Bradford Davis, Phil Peregino, and Phil Hufnal

ARL-TR-6790 **January 2014**

NOTICES

Disclaimers

The findings in this report are not to be construed as an official Department of the Army position unless so designated by other authorized documents.

Citation of manufacturer's or trade names does not constitute an official endorsement or approval of the use thereof.

Destroy this report when it is no longer needed. Do not return it to the originator.

Army Research Laboratory
Aberdeen Proving Ground, MD 21005-5069

ARL-TR-6790 **January 2014**

An Experimental Approach to Determine the Flight Dynamics of NASA's Mars Science Lab Capsule

Doug Petrick, Bradford Davis, and Phil Peregino
Weapons and Materials Research Directorate, ARL

Phil Hufnal
Bowhead Science and Technology

REPORT DOCUMENTATION PAGE	Form Approved OMB No. 0704-0188

1. REPORT DATE *(DD-MM-YYYY)*	2. REPORT TYPE	3. DATES COVERED (From - To)
January 2014	Final	January 2012–December 2012

4. TITLE AND SUBTITLE
An Experimental Approach to Determine the Flight Dynamics of NASA's Mars Science Lab Capsule

5a. CONTRACT NUMBER

5b. GRANT NUMBER

5c. PROGRAM ELEMENT NUMBER

6. AUTHOR(S)
Doug Petrick, Bradford Davis, Phil Peregino, and Phil Hufnal*

5d. PROJECT NUMBER
AH80

5e. TASK NUMBER

5f. WORK UNIT NUMBER

7. PERFORMING ORGANIZATION NAME(S) AND ADDRESS(ES)
U.S. Army Research Laboratory
ATTN: RDRL-WML-F
Aberdeen Proving Ground, MD 21005-5069

8. PERFORMING ORGANIZATION REPORT NUMBER
ARL-TR-6790

9. SPONSORING/MONITORING AGENCY NAME(S) AND ADDRESS(ES)
National Aeronautics and Space Administration
300 E. St., SW
Washington, DC 20546

10. SPONSOR/MONITOR'S ACRONYM(S)
NASA

11. SPONSOR/MONITOR'S REPORT NUMBER(S)

12. DISTRIBUTION/AVAILABILITY STATEMENT
Approved for public release; distribution is unlimited.

13. SUPPLEMENTARY NOTES
*Bowhead Science and Technology, 4900 Seminary Road, Suite 1200, Alexandria, VA 22311

14. ABSTRACT
This report details the innovative method used to experimentally capture the flight dynamics of the atmospheric entry shape of NASA's Mars Science Laboratory (MSL) capsule. This approach uses a large-caliber high-energy gun to launch a saboted package containing a subscale MSL-shaped flight body that was highly instrumented with inertial, magnetic, and pressure sensors. The U.S. Army Research Laboratory (ARL) was responsible for the design and development of instrumented MSL Pressure Transducer Module (PTM) packages and performed the free-flight experiments at ARL's Transonic Experimental Facility at Aberdeen Proving Ground, MD. The capture, transmission, and analysis of onboard sensor data allowed the reconstruction of each trajectory and subsequent extraction of the aerodynamic coefficients. The techniques developed during this program were innovative, successfully meeting the goals of diverted flight, simulating the trajectory of the MSL capsule with instrumented MSL-PTM models, and recording flight data used for subsequent trajectory reconstruction. The method described in this report can be applied to various reentry body shapes.

15. SUBJECT TERMS
MARS, MSL, telemetry, aerodynamics, pressure, high-g, flight, trajectory, MIDAS

16. SECURITY CLASSIFICATION OF:			17. LIMITATION OF ABSTRACT	18. NUMBER OF PAGES	19a. NAME OF RESPONSIBLE PERSON
a. REPORT	b. ABSTRACT	c. THIS PAGE			Doug Petrick
Unclassified	Unclassified	Unclassified	UU	46	19b. TELEPHONE NUMBER (*Include area code*) 410-306-0738

Standard Form 298 (Rev. 8/98)
Prescribed by ANSI Std. Z39.18

Contents

List of Figures

List of Tables

Acknowledgments

The authors want to acknowledge Mark Schoenberger, NASA Langley Research Center, for his technical oversight and for funding this effort, and Rafael Lugo and Robert Tolson, North Carolina State University, for their contributions to the NASA Mars Science Laboratory trajectory reconstruction and postdata analysis. The authors also wish to thank the following personnel for their time, effort, and support in preparing and conducting the aeroballistic experiments: Bernie Guidos, U.S. Army Research Laboratory (ARL), for experiment management and execution; Ken McMullen, U.S. Army Testing Center (ATC), for telemetry acquisition; Kenneth Pugh, Dynamic Science Incorporated/Bowhead Science and Technology (DSI/Bowhead), for MIDAS and pressure board assembly and calibration; Kevin Witkowski, Bobby Hall, Brad Ludwig (ARL), and Pete Jones (DSI/Bowhead) for model fabrication; Walt Zdon (ATC) for radar data capture and reduction; Martin Chidsey (ATC) for flight follower video capture; Rick Moore, Lester Hitch, and Rashad Scott, Advanced Design Manufacturing, for rapid prototyping and fabrication of sabots; and the entire ARL Transonic Experimental Facility gun crew (Bill Aubry, Barry Hudler, John Heath, Jared Kranz, Eric Miller, and Kenneth Willan). The authors also appreciate Moshe Hamaoui for his technical review of this report.

INTENTIONALLY LEFT BLANK.

1. Introduction

The U.S. Army Research Laboratory (ARL), Guidance Technologies Branch (GTB), has partnered with National Aeronautics and Space Administration (NASA) Langley Research Center (LaRC) on several occasions to conduct free-flight experiments of instrumented bodies with embedded sensors to obtain aerodynamic data. Under previous NASA efforts from 2006 through 2009, ARL successfully conceived, developed, and launched subscale versions of the Apollo-shaped command module and later the Orion-shaped Crew Exploration Vehicle (CEV) (*1*). The instrumented subscale models transmitted acceleration, angular rate, magnetic angle, and pressure data during the flight experiments with ARL's Multifunctional Instrumentation and Data Acquisition System (MIDAS) (*2*). ARL worked with NASA LaRC and their subcontractors to reconstruct the trajectories and define the aerodynamics (*3, 4*). For this latest effort, NASA challenged ARL to conduct free-flight experiments of subscale models of the Mars Science Lab (MSL) capsule to empirically simulate the space vehicle's entry into the Martian atmosphere. The MSL capsule is a heat shield entry vehicle that serves to protect the Curiosity rover as it enters the Martian atmosphere (see figure 1).

Figure 1. MSL capsule rendering.

NASA and ARL worked together to develop an instrumented model to be fired from the 178-mm-diameter (7-in) High Altitude Research Project (HARP) gun. The maximum diameter was 178 mm with the sabot included, but the actual subscale model diameter was 171 mm. The 178-mm gun was built for HARP, which was started in the 1960s to characterize atmosphere conditions at high altitudes and continues to be used today (*5, 6*). The free-flight subscale model was based on NASA specifications so that its flight behavior would closely replicate the full-scale MSL capsule. The data required included tracking radar velocity and position information

combined with inertial measurement unit (IMU) flight data that included pressure transducer readings. The pressure transducers were embedded within the forward facing “heat shield” of the body. While in flight, the onboard MIDAS telemetry module (TM) transmitted the sensor data to a ground recording system. The postflight trajectory, aerodynamic, and atmospheric reconstruction techniques used for the 2012 MSL mission include extended Kalman filter and Kalman-Schmidt. These methods of reconstruction are being tested and refined in part by using the Aberdeen Proving Ground (APG), MD, range (*7*).

2. Uninstrumented 100-mm Subscale Models

2.1 Lift Force Due to CG Offset

A lift force is created because of the orientation of the body in flight due to the offset of its CG. The free-body diagram of the lifting MSL body with axis of symmetry is shown in figure 2. In bore and in flight, the vehicle flies heat shield first, with the CG offset positioned above the axis of symmetry. The resulting trajectory of the gun-launched model replicates the entry flight dynamics of the actual MSL capsule. The CG must not spin out of vertical orientation or the lifting force vector will not remain parallel and opposite to the gravity vector.

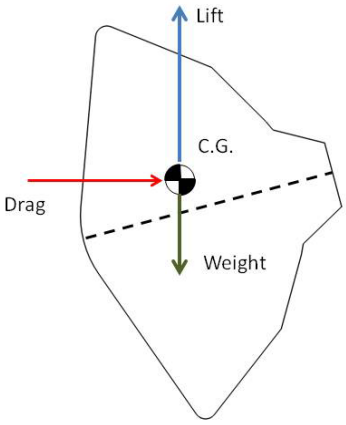

Figure 2. Lifting MSL free-body diagram.

2.2 Development Method

2.2.1 Scaling

The maximum diameter of the forward heat shield body was sized to 100 mm so it could be saboted and fired from a 120-mm gun. Knowing the CG location of the 171-mm models, as specified by NASA, the CG locations of the 100-mm models were scaled linearly with the change in diameter. With the exterior geometry defined, one design parameter remained: determining the mass of the 100-mm model. To do so, we want the 100-mm model to have the

same acceleration history as the 171-mm model. Assuming the same initial velocity and identical aerodynamic coefficients for the 100-mm model and the 171-mm model, the mass-to-diameter ratio is attained by using the following equations:

$$C_D = \frac{F_D}{\frac{1}{2}\rho V^2 S} \tag{1}$$

$$F_D = \left(\frac{1}{2}\rho V^2 C_D\right)(S) \tag{2}$$

$$F = ma \tag{3}$$

$$a_D = \left(\frac{1}{2}\rho V^2 C_D\right)\left(\frac{S}{m}\right) \tag{4}$$

$$a_{D_{120\,mm}} = a_{D_{7\,in}} \tag{5}$$

$$S = \pi \frac{d^2}{4} \tag{6}$$

$$\frac{d_{120mm}}{m_{120mm}} = \frac{d_{7in}}{m_{7in}} \tag{7}$$

where C_D = drag coefficient, F_D = drag force, P = density, V = velocity, S = effective area, D = heat shield diameter, M = mass, and a = acceleration.

Rearranging equation 1 to solve for the C_D yields equation 2. Setting the forces in equation 2 and equation 3 equal to one another and solving for acceleration gives equation 4. This is the acceleration as a function of drag force parameters, effective area, and mass. Next, set the acceleration of the 100-mm model equal to that of the 171-mm model (equation 5). S in equation 6 is dependent on the diameter of the heat shield. Knowing the mass of the 171-mm model, its effective area, and the effective area of the 100-mm model, the mass of the 100-mm model can be found. Since effective area depends upon the diameter, the following mass-to-diameter ratio is established (equation 7) for scaling the models. The mass of the 171-mm model was found from the computer-aided design (CAD) model because no hardware had been machined at this point. The CAD model includes all material densities, including those of potting and electronic boards.

2.2.2 CG Positioning

The least expensive and easiest way to produce these models would have been to machine them out of one piece of steel. Based on the diameter and shape of the model, however, we couldn't obtain our desired mass or CG location with a single solid-steel body. To shift the CG in a model, two things can be done: (1) remove material to create a void centered along the axis opposite to where the CG should be located and (2) remove material of one density and replace it with material of a different density. To create the nonaxisymmetric weight distribution and also meet the mass requirement, a multibody, multimaterial structure was required. The model has an AISI 12L14 hot-rolled steel outer body that includes four WMiCu class 1 tungsten alloy ballasts (see figure 3).This tungsten alloy has a density of 0.614 lb/in^3 (17 g/cm^3) compared with 12L14 steel, which has a density of 0.284 lb/in^3 (7.86 g/cm^3). The 12L14 body has pockets where the subtraction of steel and addition of tungsten ballasts locates the CG off axis in the direction of the tungsten ballasts (figure 3). A 51-mm-diameter (2-in) tungsten tail was also required to increase the overall mass (figure 3). Beneath the tungsten tail there is a pocket void (figure 4). The tungsten tail shifted the CG farther back from the nose along the axial direction (x-axis). A groove was cut by Electrical Discharge Machining along the outside cylindrical surface of the ballasts to allow air to press out as the ballasts were installed. The tungsten inserts were installed by thermal shrink fitting. Once installed, the tungsten was machined with the steel to achieve a smooth contour (figure 5). They were painted with red and black sections prior to any flight experiment.

For the 171-mm model, tungsten accounted for 32% of total weight, and for the 100-mm model, tungsten accounted for 51% of total weight. It was increasingly difficult to meet the mass requirements for smaller-scale models because mass scales with effective area and effective area scales with the radius squared. A smaller-scale model with a radius equal to one-half the full-scale radius has a quarter of the effective area and a quarter of the mass. If one scaled by volume (instead of effective area), the mass would be reduced by a cubic function. The half-scale model would then have an eighth of the full-scale mass. The effective area scaling made it extraordinarily difficult to fit the required mass into so small a volume, but this was necessary to match the trajectory of the 100-mm model to the 171-mm model.

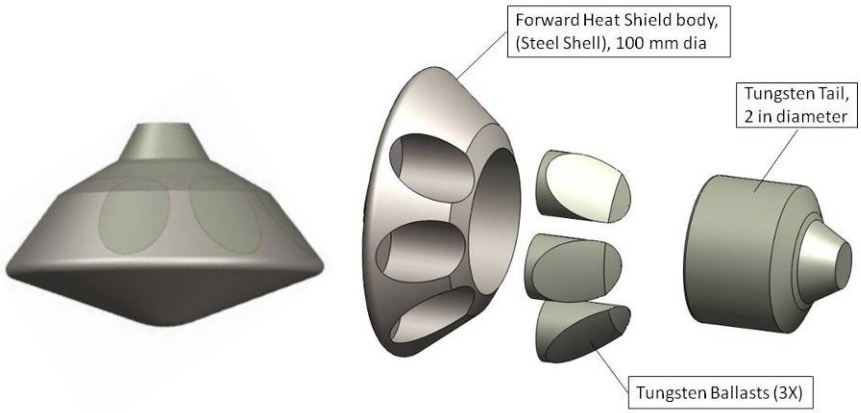

Figure 3. Heat shield and tungsten inserts.

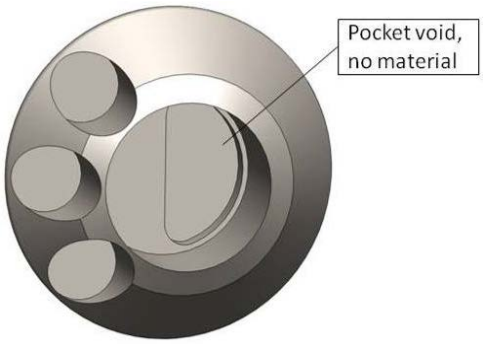

Figure 4. Heat shield showing the pocket void.

Figure 5. 100-mm MSL machined hardware.

2.3 Measured Mass Properties

There was negligible error between the desired, calculated (via SolidWorks CAD), and measured mass, CG, and moment of inertia (MOI), as seen in tables 1 and 2. Only the mass and CG locations were being matched, as MOI was not a criterion for the design process. The actual

measurements were taken using the Space Electronics CG measurement and MOI measurement machine at the Transonic Experimental Facility (TEF) located at APG.

Table 1. Mass and CG measurements.

Measurement	Mass (kg [lb])	X-CG (mm [in])	Y-CG (mm [in])	Z-CG (mm [in])
Desired	2.54 [5.61]	29.97 [1.180]	0.00 [0.000]	2.16 [0.085]
Calculated	2.55 [5.63]	28.85 [1.136]	0.00 [0.000]	2.16 [0.085]
MSL 3 measured	2.54 [5.60]	28.85 [1.136]	–0.05 [-.002]	2.08 [0.082]
MSL 4 measured	2.54 [5.60]	29.24 [1.151]	–0.15 [-.006]	2.01 [0.079]
MSL 5 measured	2.54 [5.59]	28.91 [1.138]	–0.03 [-.001]	1.91 [0.075]
MSL 6 measured	2.53 [5.57]	28.96 [1.140]	–0.10 [-.004]	2.06 [0.081]

Table 2. MOI measurements.

Measurement	Ixx ($kg\text{-}m^2$ [$lb\text{-}in^2$])	Iyy ($kg\text{-}m^2$ [$lb\text{-}in^2$])	Izz ($kg\text{-}m^2$ [$lb\text{-}in^2$])
Desired	NA	NA	NA
Calculated	1.866×10^{-3} [6.375]	1.318×10^{-3} [4.503]	1.256×10^{-3} [4.293]
MSL 3 measured	1.900×10^{-3} [6.492]	1.371×10^{-3} [4.686]	1.280×10^{-3} [4.375]
MSL 4 measured	1.924×10^{-3} [6.576]	1.351×10^{-3} [4.616]	1.300×10^{-3} [4.444]
MSL 5 measured	1.883×10^{-3} [6.433]	1.362×10^{-3} [4.654]	1.286×10^{-3} [4.394]
MSL 6 measured	1.871×10^{-3} [6.394]	1.336×10^{-3} [4.566]	1.379×10^{-3} [4.712]

2.4 Sabot and Pusher Plate Design

The requirements for the sabot and pusher plate were two-fold: (1) maintain a predefined in-bore orientation prior to flight and (2) provide a seal against gun gasses. The flight body is enclosed by four interlocking sabot petals, each with a unique cavity intended to contain the MSL body geometry. There were two variants of the sabot trim angle: (1) one that keeps the flight body at zero trim, with its axis parallel to the gun axis and (2) one that orients the flight body at a trim angle with a known pitch angle at muzzle exit. Both sabot versions feature four petals that fit together with a uniform interlocking-teeth surface. As in previous instrumented CEV flight experiments, the sabots were glass-filled nylon produced by the selective laser sintering process. A nylon pusher plate at the base keeps the four petals interlocked and seals the launch package within the gun bore. Figure 6 is an example of an MSL that was preoriented in a lifting sabot. The black line drawn on the center of the painted red section indicates the location of the weight offset. In bore, the weight is positioned vertically up so that the lift would be in the vertical direction (figure 7). The 120-mm sabots were different from the 178-mm sabots in scale only; the material and design were the same.

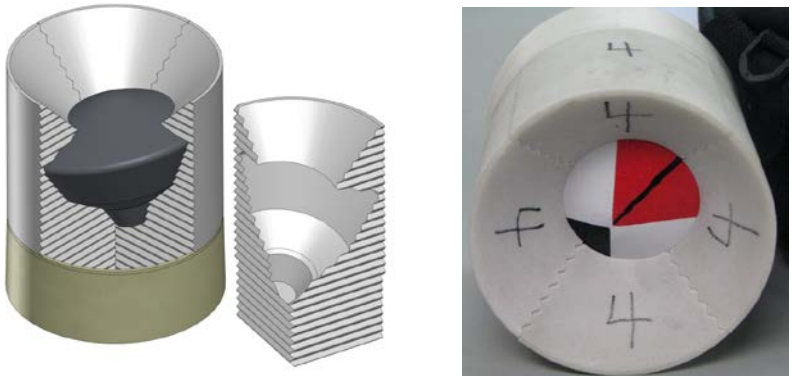

Figure 6. Lifting 100-mm MSL in a preangled sabot.

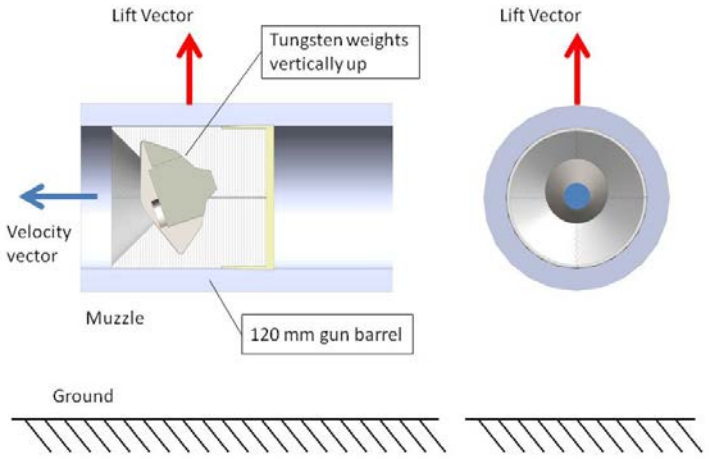

Figure 7. Free-body diagram.

2.5 Experimental Results

2.5.1 Sabot Separation Experiment

Before launching the lifting bodies, there was a series of flight experiments using the nonlifting MSL models to determine sabot separation performance. The nonlifting models have an axisymmetric weight distribution because they do not feature the three offset tungsten ballasts. The nonlifting bodies were painted with black and white sections (figure 8). For the axisymmetric sabot, the projectile's centerline is oriented so that it is parallel to the gun tube axis. The models were launched from the smoothbore 120-mm M256 tank gun with a 3.05-m (10-ft) extension at TEF, and sabot separation was successfully verified (figure 9). This approach of developing axisymmetric nonlifting MSL flight bodies to verify sabot separation performance was also implemented for the 171-mm models.

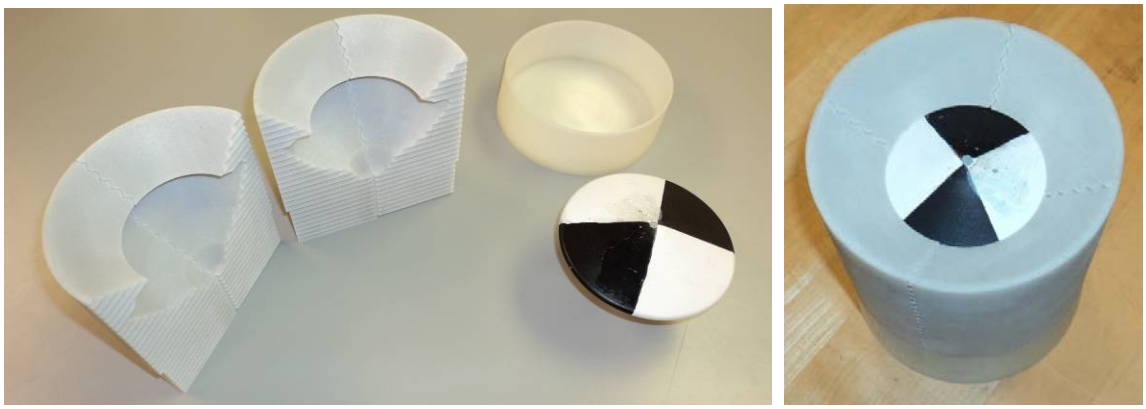

Figure 8. Nonlifting 100-mm MSL assembled in a zero-angled sabot.

Figure 9. M256 gun.

2.5.2 Phase 1 Tracking Radar Flight Experiment

The next step was to verify that the radar could track a lifting MSL body. Phase 1 experiments involved launching six cylindrical slugs and one MSL model, as seen in the table 3 firing log. The ARL-developed cylindrical projectiles were low-cost surrogates that were used to replicate the trajectories of the NASA capsules (*8*). These cylindrical slugs were nylon with steel inserts at various radial offsets from the centerline (figure 10). The level of lift depended on the radial offset of the steel insert from the centerline; the greater the offset, the higher the lift. These were categorized by zero-lift (cyl-0L), medium-lift (cyl-ML), and high-lift (cyl-HL) slugs. Figure 11 shows one of the high-lift cylinders after successfully being launched and lifting as intended.

The Weibel tracking radar antenna was set up 42 m behind the gun and a few meters to the right of it (figure 8). The tracking radars must follow a flight body that can swerve very quickly. The plot below was generated from a NASA trajectory simulation of lifting 100-mm MSL models and shows a steep change in altitude of nearly 700 m over its first 900 m of downrange distance (figure 12). The tracking radar antenna can be seen behind the yellow saw horse. The radar quadrant elevation (QE) was adjusted during the experiment. Of those six cylinders, the radar locked onto only one, the zero-lift cylindrical slug. Unfortunately, the radar was unable to lock onto the others. The MSL launch package survived launch and the four petals separated properly,

as seen by high-speed video recording. The high-speed video showed that the cylinders veered off to the right. It was proposed that in-bore spinning had caused the CG—and hence the lift vector—to rotate out of vertical. If true, the model would indeed veer to the side. The last shot of phase 1 was deliberately rotated out of vertical to off-set spin-up such that the CG would be vertical at muzzle exit. If spin up occurred in this situation, then the model should lift upward initially. The final shot of phase 1 showed negligible cross-range motion, confirming the presence of in-bore rotation.

Table 3. 120-mm gun phase 1 tracking radar flight experiment firing log.

Date	Shot	TEF #	Config.	In-bore Mass (kg)	Flight Mass (kg)	Charge Mass (kg)	Expected Velocity (m/s)	Expected Mach	Radar QE (°)	Radar Unlock (ms)	Lock On?
27 March 2012	1	38361	Cyl-0L	3.23	3.23	4.5	1200	3.5	12.5	600	Y
—	2	38362	Cyl-ML	3.23	3.23	4.5	1200	3.5	12.5	600	N
—	3	38363	Cyl-ML	3.23	3.23	4.5	1200	3.5	17	600	N
—	4	38364	Cyl-ML	3.23	3.23	4.5	1200	3.5	25	600	N
—	5	38365	MSL-3	4.02	2.54	5.3	1424	4.3	20	600	N
28 March 2012	6	38366	Cyl-HL	3.23	3.23	3.0	1020	3.0	10	200	N
—	7	38367	Cyl-HL	3.23	3.23	3.0	1020	3.0	10	200	N

Figure 10. ARL high-lift cylindrical slug.

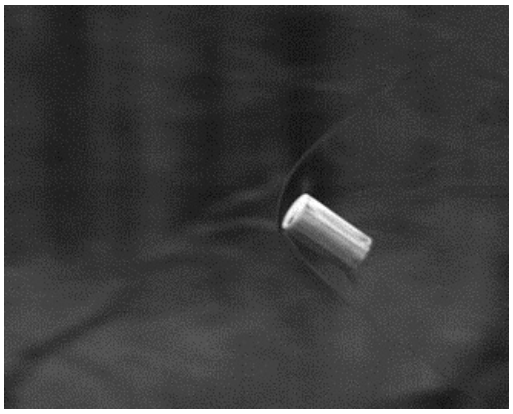

Figure 11. High-speed flight follower showing high-lifting cylinder.

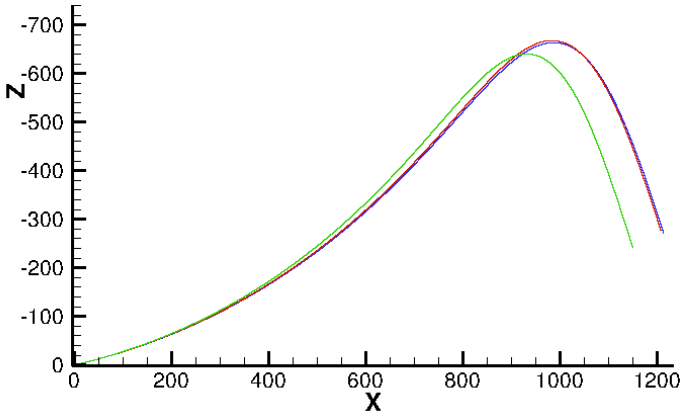

Figure 12. MSL simulated trajectories.

2.5.3 Phase 2 Tracking Radar Flight Experiment

The poor results in phase 1 required some changes. Phase 2 involved adjusting the gun and radar QE to maximize the time that the lifting shots were inside the radar beam (table 4). This time, all cylindrical slugs were successfully tracked. For the next two MSL shots, the radar did not lock on. High-speed video indicated that the shots did not climb as intended. Based on these observations, the last MSL model (MSL-6) was prematurely rotated out of vertical so that as the sabot package travelled down the tube that would orient the CG offset in the vertical position. The tracking radar successfully followed the trajectory of the last MSL lifting body. The tracking radar data for that shot is plotted in figure 13. The model climbed to approximately 400 m in altitude and traveled 1200 m in range. This differed from the simulated trajectory shown in figure 12. The differences can be attributed to the model lifting out of vertical plane and into the horizontal plane, which was not shown.

Table 4. 120-mm gun phase 2 tracking radar flight experiment firing log.

Date	Shot	TEF#	Config.	In-bore Mass (kg)	Flight Mass (kg)	Charge Mass (kg)	Velocity (m/s)	Mach	Radar QE (°)	Radar Unlock (ms)	Lock on?
17 April 2012	1	38380	Cyl-ML	3.23	3.23	3.0	808	2.4	10	150/200	Y
—	2	38381	Cyl-ML	3.23	3.23	3.75	1019	3.0	9	150/200	Y
—	3	38382	Cyl-ML	3.23	3.23	4.77	1152	3.4	8.5	150/200	Y
—	4	38383	Cyl-HL	3.23	3.23	3.75	966	2.8	8.5	200/250	Y
18 April 2012	5	38384	Cyl-HL	3.23	3.23	4.77	1231	3.6	8.5	200/250	Y
—	6	38385	Cyl-HL	3.23	3.23	5.00	1236	3.6	9.5	200/250	Y
—	7	38386	MSL-4	4.04	2.54	5.3	1140	3.4	9.5	200/250	N
—	8	38387	MSL-5	4.05	2.54	4.6	1083	3.2	15	200/250	N
—	9	38388	MSL-6	4.00	2.53	4.6	1050	3.1	9.5	200/250	Y

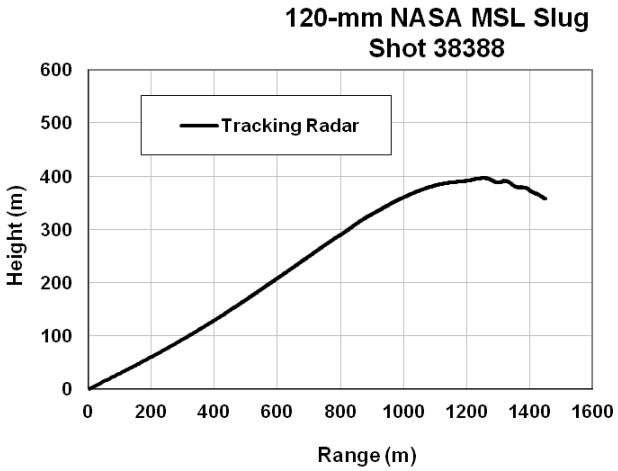

Figure 13. Height vs. range from tracking radar for lifting MSL-6 flight body.

3. Instrumented 171-mm Subscale Models

3.1 Mechanical Design

The next challenge was to develop the instrumented MSL-Pressure Transducer Module (PTM) models. There were three mechanical design objectives.

(1) Obtain the desired physical properties for the instrumented flight body.

(2) Integration of pressure sensors.

(3) Integration of the stand-alone MIDAS TM.

3.1.1 Mass Properties

To meet the weight and CG requirements, the instrumented model was split into multiple bodies of three different materials (figure 14). The tungsten upper cap moved the CG farther back from the nose along the axis of symmetry. The nose cone and transducer section are lightweight and thus shift the CG away from the nose of the heat shield. These two parts also allowed for pressure sensor integration. Therefore, the nose cone and transducer section are two separate bodies made of aluminum. The CG positioning procedure, as described in section 2, was used to shift the CG off the axis of symmetry. The 304 stainless steel midsection houses the MIDAS TM and locates two tungsten ballasts 33.83 mm (1.332 in) in diameter. The two tungsten ballasts shifted the CG off the X-axis (axis of symmetry) in the negative Z-axis direction. The flight-body coordinate system as defined by NASA is shown in figure 15. The midsection also features holes on the positive Z-axis, which along with the tungsten ballasts achieve the desired CG offset in the negative Z direction.

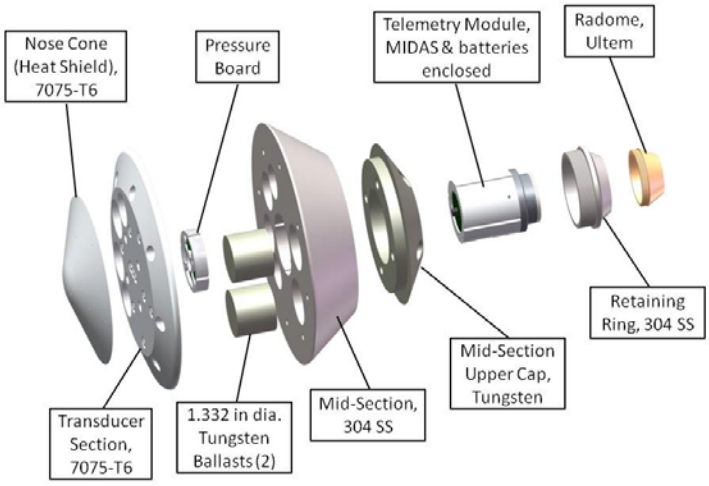

Figure 14. MSL-PTM CAD model assembly shown in exploded view.

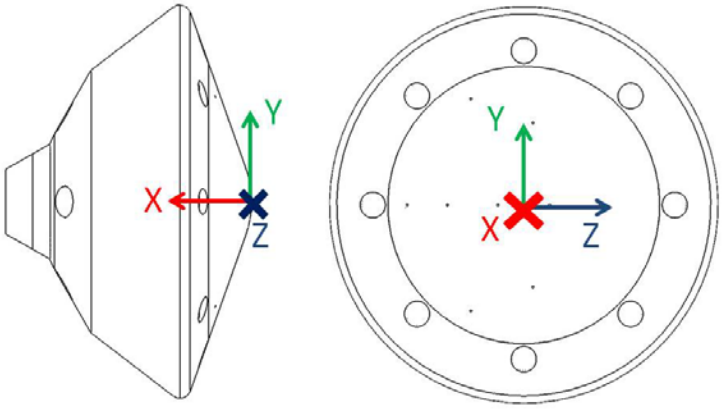

Figure 15. MSL-PTM coordinate system

The desired CG location defined by NASA was verified by the CAD model calculation. Measurements of the fully assembled and potted models were made at TEF using the Space Electronics CG measurement machine. All measurements were within the acceptable range as determined by NASA (tables 5 and 6).

Table 5. MSL-PTM mass and CG measurements.

MSL-PTM 6				
Measurement	**Mass (kg [lb])**	**X-CG (mm [in])**	**Y-CG (mm [in])**	**Z-CG (mm [in])**
NASA specified target	NA	51.44 [2.025]	0.00 [0.000]	–3.68 [–0.145]
Calculated	7.47 [16.46]	51.38 [2.023]	0.00 [0.000]	–3.71 [–0.146]
Measured	7.35 [16.21]	52.12 [2.052]	–0.08 [–0.003]	–3.86 [–0.152]
Difference[a]	0.11 [0.25]	0.74 [0.029]	0.08 [0.003]	0.18 [0.007]

MSL-PTM 7				
Measurement	**Mass (kg [lb])**	**X-CG (mm [in])**	**Y-CG (mm [in])**	**Z-CG (mm [in])**
NASA specified target	NA	51.44 [2.025]	0.00 [0.000]	–3.68 [-0.145]
Calculated	7.47 [16.46]	51.38 [2.023]	0.00 [0.000]	–3.71 [-0.146]
Measured	7.37 [16.24]	51.87 [2.042]	0.13 [0.005]	–3.71 [-0.146]
Difference[a]	0.10 [0.22]	0.43 [0.017]	0.13 [0.005]	0.03 [0.001]

MSL-PTM 8				
Measurement	**Mass (kg [lb])**	**X-CG (mm [in])**	**Y-CG (mm [in])**	**Z-CG (mm [in])**
NASA specified target	NA	51.44 [2.025]	0.00 [0.000]	–3.68 [–0.145]
Calculated	7.47 [16.46]	51.38 [2.023]	0.00 [0.000]	–3.71 [–0.146]
Measured	7.37 [16.24]	52.07 [2.050]	0.15 [0.006]	–3.86 [–0.152]
Difference[a]	0.10 [0.22]	0.64 [0.025]	0.15 [0.006]	0.18 [0.007]

[a]Note: Difference is absolute value of target measured.

Table 6. MSL-PTM moment of inertia measurements.

MSL-PTM 6			
Measurement	**Ixx ($kg\text{-}m^2$ [$lb\text{-}in^2$])**	**Iyy ($kg\text{-}m^2$ [$lb\text{-}in^2$])**	**Izz ($kg\text{-}m^2$ [$lb\text{-}in^2$])**
Calculated	1.927×10^{-2} [65.85]	1.215×10^{-2} [41.52]	1.193×10^{-2} [40.75]
Measured	1.899×10^{-2} [64.90]	1.260×10^{-2} [43.05]	1.228×10^{-2} [41.95]

MSL-PTM 7			
Measurement	**Ixx ($kg\text{-}m^2$ [$lb\text{-}in^2$])**	**Iyy ($kg\text{-}m^2$ [$lb\text{-}in^2$])**	**Izz ($kg\text{-}m^2$ [$lb\text{-}in^2$])**
Calculated	1.927×10^{-2} [65.85]	1.215×10^{-2} [41.52]	1.193×10^{-2} [40.75]
Measured	1.902×10^{-2} [65.00]	1.259×10^{-2} [43.02]	1.227×10^{-2} [41.92]

MSL-PTM 8			
Measurement	**Ixx ($kg\text{-}m^2$ [$lb\text{-}in^2$])**	**Iyy ($kg\text{-}m^2$ [$lb\text{-}in^2$])**	**Izz ($kg\text{-}m^2$ [$lb\text{-}in^2$])**
Calculated	1.927×10^{-2} [65.85]	1.215×10^{-2} [41.52]	1.193×10^{-2} [40.75]
Measured	1.905×10^{-2} [65.10]	1.260×10^{-2} [43.04]	1.2280^{-2} [41.98]

3.1.2 Pressure Sensor Integration

Ten pressure sensors were integrated into each MSL-PTM model. All 10 transducers received input from vented port holes on the forward-facing heat shield (figure 16). The models were launched with their heat shield facing forward to replicate entry conditions of the full-scale MSL capsule. The transducers were to monitor the pressures on the heat shield throughout the flight. The heat shield was composed of two sections, the nose cone and transducer plate. The purpose of this two-part concept was for ease of machining and assembly. The transducers were oriented parallel to the axis of symmetry, mounted in the transducer section behind the aluminum nose cone section. The 10 ports in the nose cone were 1 mm in diameter. The porthole locations in the instrumented MSL scale model were scaled to the identical locations in the actual MSL capsule. The locations of the portholes are shown in figure 17.

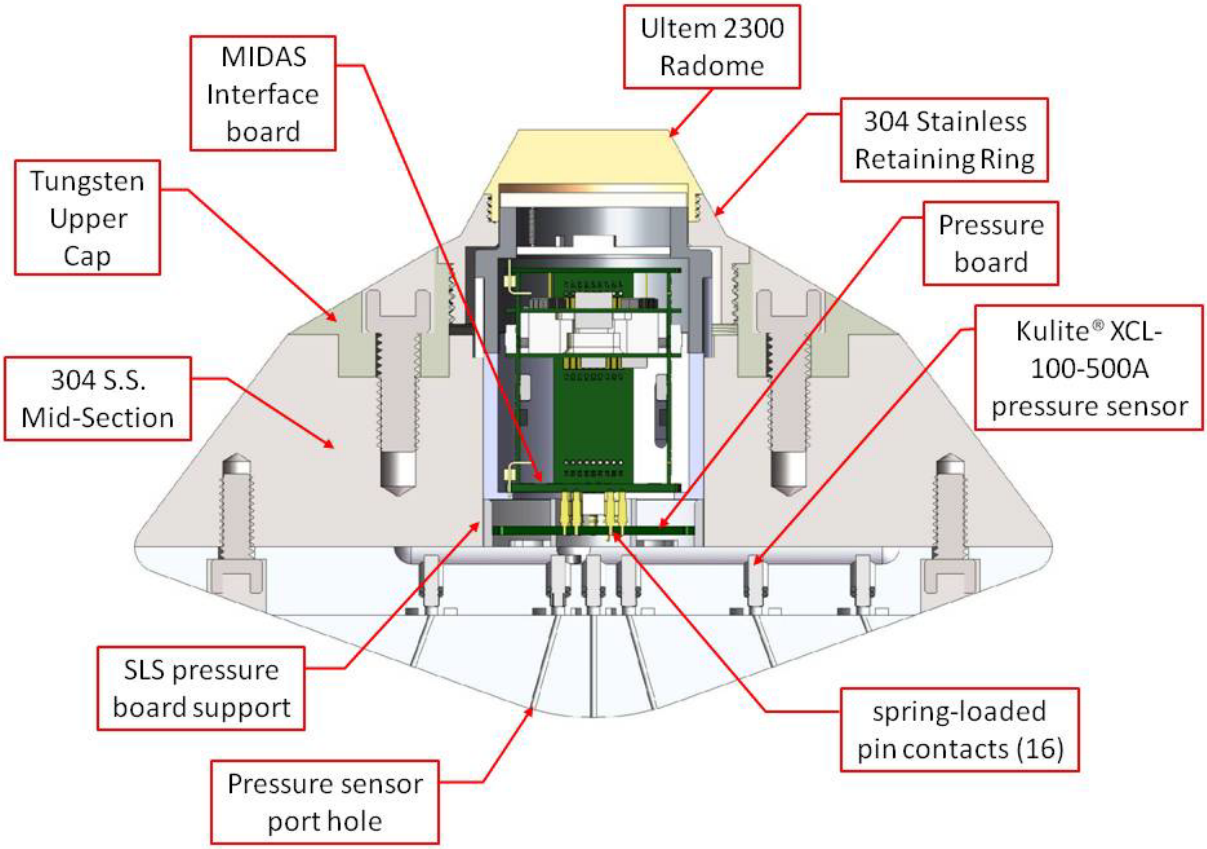

Figure 16. MSL-PTM cutaway diagram.

Figure 17. MSL-PTM pressure port locations.

The 2.56-mm-diameter (0.101 in) by 9.52-mm-long (3/8 in) pressure transducers used were Kulite* XCL-100-500A (rated for 3447-kPa [500-psi] absolute pressure). The transducer section had specially machined mounting holes into which the transducers were installed with two o-rings with a 2.5-mm inner diameter and 1-mm thickness (figures 18 and 19). The transducers leads were then soldered to the pressure board (figure 20). The pressure board was used to power the transducers and perform temperature compensation for each transducer signal channel. The pressure board had 16 spring-loaded pin contacts to route pressure signals to the MIDAS and get power from the MIDAS batteries. The MIDAS board stack had landing pads for the spring-loaded pin contacts, which depress once the MIDAS is installed into the model. The pins were located on the pressure board so that acceleration forces during launch keep the pins pressed up against the MIDAS. The pressure board was secured in place in a support made from selective laser sinter (SLS) material (figure 21, left). The SLS support was secured to the transducer section, with careful attention to angular alignment. The image on the right in figure 21 shows the pressure board potted and installed within the model, as it appeared with the MIDAS TM removed.

* Kulite is a registered trademark of Kulite Semiconductor Products, Inc., Leonia, NJ.

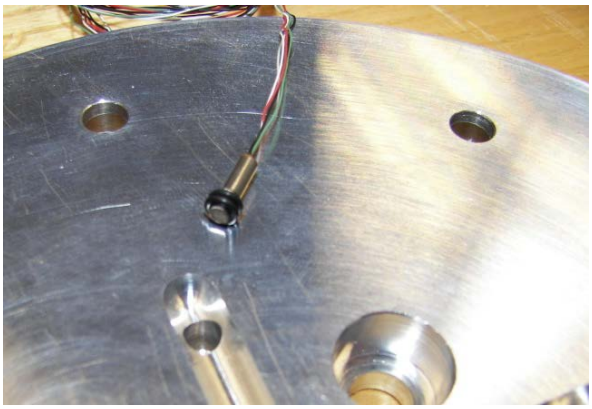

Figure 18. Kulite XCL-100-500A pressure sensor near transducer section mounting hole.

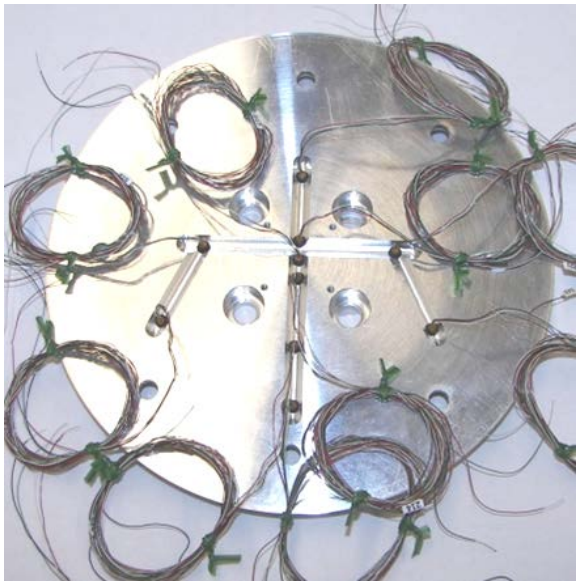

Figure 19. All 10 pressure sensors installed into the transducer section.

Figure 20. Pressure sensors wired to custom-designed pressure board.

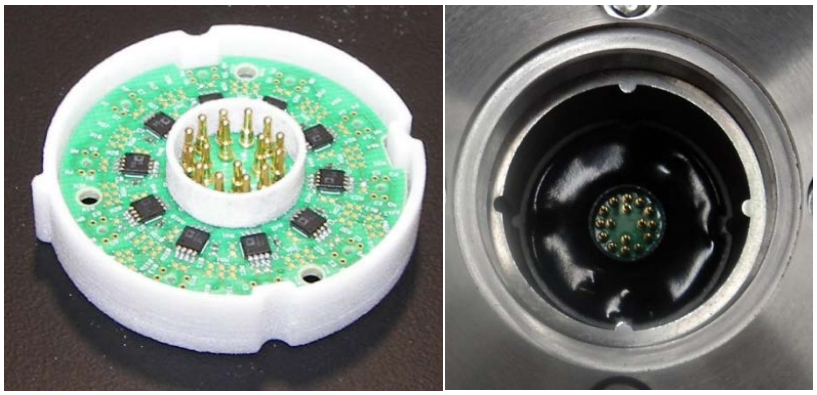

Figure 21. Pressure board in its SLS support (left) and after potted installation (right).

3.1.3 MIDAS Integration

The MIDAS TM includes the board stack with rechargeable power supply, an S-band transmitter, and antenna (figures 22 and 23). As seen in figure 17, the stand-alone MIDAS TM is located toward the aft end of the model. The MIDAS TM has an aluminum body with exterior geometry machined by electrical discharge machining. The TM housing is keyed to ensure proper alignment of the MIDAS coordinate system with flight body coordinate system (figure 23). Based on the results of the previous CEV-PTM experiments, the MSL-PTM IMU sensor complement used redundant magnetometers, accelerometers, and rate gyros for measuring motion in the axial, pitch, and roll orientations. MIDAS is able to telemeter 32 channels of data. Table 7 shows the measurement outputs from the MIDAS. To turn on the module, a four-lead low-profile jumper is inserted into a connector at the bottom of the module (figure 23, right).

The MIDAS TM slides down onto the push pins of the pressure board. A 304 stainless steel retaining ring threads down onto the shoulder of the MIDAS and keeps it securely pressed up against the electrical push pin contacts. A radio frequency (RF) transparent radome, made from Ultem* 2300, threads into the retaining ring.

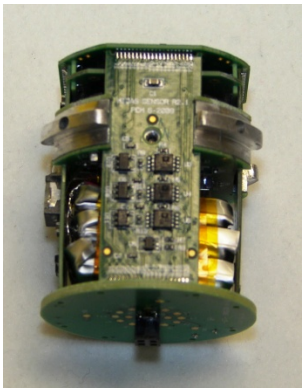

Figure 22. MIDAS electronics board stack.

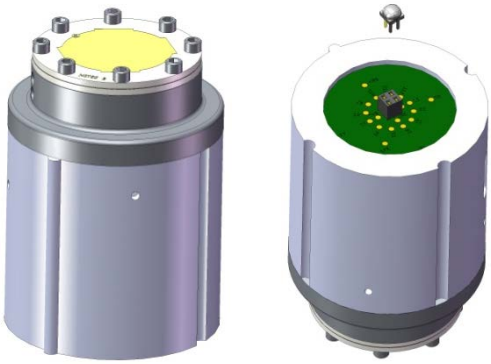

Figure 23. Packaged MIDAS TM.

* Ultem is a registered trademark of SABIC Innovative Plastics Holding BV, Pittsfield, MA.

Table 7. MIDAS measurement outputs.

Part	Measurement	Bandwidth	Range	Label
ADXSTC3-HG	Axial acceleration along I	10 KHz	+/–10 Kg	Acc_I1
AD22283	Axial acceleration along I	10 KHz	+/–250 g	Acc_I2
AD22284	Radial acceleration along J	10 KHz	+/–35 g	Acc_J1
AD22284	Radial acceleration along J	10 KHz	+/–35 g	Acc_J2
AD22284	Radial acceleration along K	10 KHz	+/–35 g	Acc_K1
AD22284	Radial acceleration along K	10 KHz	+/–35 g	Acc_K2
HMC1023	Magnetic field along I	10 KHz	+/–1.5 Gauss	Mag_I1
HMC1023	Magnetic field along J	10 KHz	+/–1.5 Gauss	Mag_J1
HMC1023	Magnetic field along K	10 KHz	+/–1.5 Gauss	Mag_K1
HMC1023	Magnetic field along I	10 KHz	+/–1.5 Gauss	Mag_I2
HMC1023	Magnetic field along J	10 KHz	+/–1.5 Gauss	Mag_J2
HMC1023	Magnetic field along K	10 KHz	+/–1.5 Gauss	Mag_K2
ADXRS300	Rate about I	10 KHz	+/–400 deg/s	Rate_I1
ADXRS300	Rate about J	10 KHz	+/–2000 deg/s	Rate_J1
ADXRS300	Rate about J	10 KHz	+/–2000 deg/s	Rate_J2
ADXRS300	Rate about K	10 KHz	+/–2000 deg/s	Rate_K1
ADXRS300	Rate about K	10 KHz	+/–2000 deg/s	Rate_K2
AD22284 (4 each)	Roll rate from accelerometers	10 KHz	+/–5 Hz	AO_Sum
XCL-100	Pressure at location 1	10 KHz	–100 to 500 psi	Pressure_1
XCL-100	Pressure at location 2	10 KHz	–100 to 500 psi	Pressure_2
XCL-100	Pressure at location 3	10 KHz	–100 to 500 psi	Pressure_3
XCL-100	Pressure at location 4	10 KHz	–100 to 500 psi	Pressure_4
XCL-100	Pressure at location 5	10 KHz	–100 to 500 psi	Pressure_5
XCL-100	Pressure at location 6	10 KHz	–100 to 500 psi	Pressure_6
XCL-100	Pressure at location 7	10 KHz	–100 to 500 psi	Pressure_7
XCL-100	Pressure at location 8	10 KHz	–100 to 500 psi	Pressure_8
XCL-100	Pressure at location 9	10 KHz	–100 to 500 psi	Pressure_9
XCL-100	Pressure at location 10	10 KHz	–100 to 500 psi	Pressure_10
Li battery	Transmitter voltage	10 KHz	0-5V	10 KHz

3.2 Pressure Sensor Calibration

Calibration of the pressure transducers was performed with the MIDAS TM powered on and installed into the MSL body. Before the MSL-PTMs were taken to NASA LaRC for the pressure calibration, they were placed in a vacuum chamber at ARL for preliminary experimentation. The purpose was not to determine the scale factors and bias of each pressure transducer, but rather ensure the electronics were functioning properly.

To obtain scale factors and bias of the 10 individual transducers, ARL used the pressure chamber at LaRC (figure 24). The chamber is a 0.197-m-diameter (7.75-in) steel cylindrical pressure vessel, featuring a glass window through which the RF signal is transmitted. The MIDAS TM was powered on, and the fully assembled model was loaded into the chamber with the antenna

facing the glass window. The chamber was pressurized to nine random pressures for about 10 s each using a design of experiments approach. Each pressure was recorded in a separate file using a ground station. The file was named after the pressure readout at the digital control.

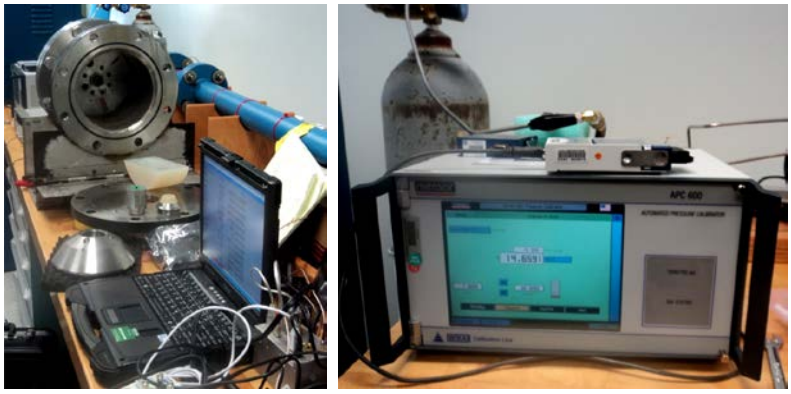

Figure 24. Pressure calibration setup.

ARL decoded the telemetry stream, found the root-mean-square bit value for the given period of recording at each pressure, and calculated scale factor and bias for each of the 10 transducers on all four MSL-PTMs. The calibration data (see appendix) was also given to NASA for its own scale factor and bias analysis. The results from ARL and NASA LaRC were in total agreement. Note that a few of the pressure transducers were not working properly.

3.3 Instrumented Flight Experiment

The flight experiments of the four MSL-PTM projectiles were completed 6–18 June 2012 using the 178-mm HARP gun at TEF (figure 25). Range equipment included high-speed flight follower video, a telemetry van, and tracking radar. The telemetry van used both fixed and tracking antennas tied to receivers and bit synchronizer/decommutation equipment to capture the flight data (figure 26). Several shots were fired before the MSL-PTM instrumented models, including ARL high-lift and zero-lift cylinders as well as MSL lifting and nonlifting bodies (figure 27). The gun QE was maintained at 12.45° and at an azimuth of 190° SSW for all flight experiments. The shot-by-shot experiment information is included in table 8.

Figure 25. 178-mm HARP gun and experimental setup.

Figure 26. Telemetry van exterior (left) and interior (right) views.

Figure 27. 178-mm cylindrical slugs and MSL-PTM models.

Table 8. 178-mm gun instrumented flight experiment firing log.

Date	Shot	TEF #	Config.	Inbore Mass (kg)	Flight Mass (kg)	Charge Mass (kg)	Velocity (m/s)	Mach
6 June 2012	1	38404	Cyl no lift	12.0	12.0	14.2	1134	3.30
	2	38405	MSL no lift	12.1	7.5	15.2	1283	3.80
7 June 2012	3	38406	Cyl no lift	12.1	12.1	14.2	1159	3.40
13 June 2012	4	38407	Cyl no lift	12.1	12.1	12.4	1060	3.12
	5	38408	MSL no lift	12.0	7.4	15.2	1277	3.76
	6	38409	MSL5PTM6 no lift	11.9	7.3	15.2	1278	3.76
14 June 2012	7	38410	MSL6PTM7 lifting	12.1	7.4	15.2	1296	3.81
18 June 2012	8	38411	MSL lifting	12.2	7.5	15.2	1276	3.75
	9	38412	MSL8PTM9 lifting	12.1	7.4	15.2	1296	3.81
	10	38413	MSL7PTM5 lifting	12.1	7.4	14.2	1242	3.65

The flight follower video from shot 2, the first uninstrumented MSL model, revealed sabot fragments following closely behind the flight body. To ensure that the sabot separated completely from the flight body, material was removed behind the radome for subsequent MSL flight body sabots. This sabot modification resulted in proper sabot separation for the first instrumented MSL-PTM (MSL5PTM6), a nonlifting flight body (figure 28). The second instrumented MSL-PTM (MSL6PTM7), a lifting flight body in an angled sabot showed significant pitching motion. Analysis of the flight follower images indicated poor sabot separation from the flight body. The sabot material ahead of the heat shield was staying on the flight body and tilting it rather than breaking away. For the third and fourth instrumented flight bodies, material was removed near the heat shield portion of the sabot to prevent this from happening again. For the fourth instrumented model, material was removed both from near the heat shield portion and behind the radome, near the rim, and cardboard shims were also added to reduce potential rotation inside the sabot (figure 29).

Figure 28. High-speed flight follower image of MSL5PTM6 followed by its sabot fragments.

Figure 29. Sabots with material removed and shims added (left) and untouched (right).

Unfortunately, one of the four MSL-PTMs (MSL6PTM7) was unable to telemeter data because the battery died while it was still in bore due to a gun misfire. It could not be extracted from the gun to turn it off because according to range safety requirements, the gun must remain idle for 30 min following a misfire. A medical evacuation also closed down range operations while this shot was in bore for an additional 15 min. The battery, which has a life of 45 min, died during the procedure to fire the gun the second time.

The tracking radar data from the three working shots are shown in figures 30 and 31. The trajectory for the axisymmetric MSL-PTM can clearly be distinguished from that of the lifting models. The roll orientation of the lifting MSL-PTMs at muzzle exit played a large part in determining their direction of drift.

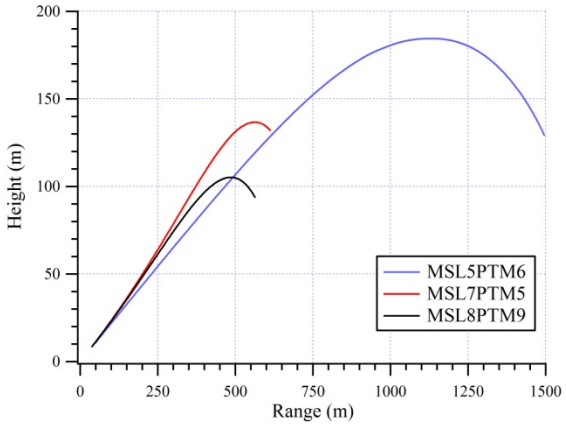

Figure 30. Height vs. range from tracking radar.

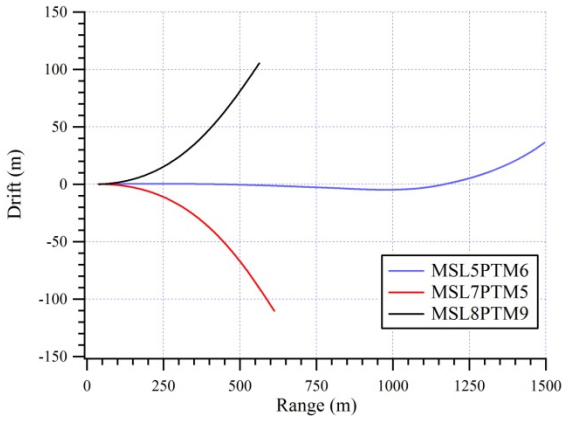

Figure 31. Drift vs. range from tracking radar.

The data from MSL5PTM6, the first instrumented flight is shown in the following figures. Figure 32 shows the in-bore launch acceleration profile. Figures 33 and 34 show the axial and radial accelerations while in flight. The magnetic aspect angle, an angle from the vehicle's principal axis to the Earth's magnetic field and denoted SigmaM, was determined from the magnetometer outputs (figure 35). The pitch, yaw, and roll rates from the angular rate sensors are shown in figures 36 and 37, and pressure data are shown in figure 38. Similar data were collected for the other two MSL-PTMs.

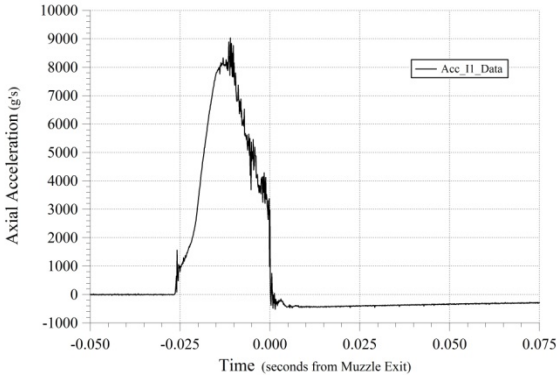

Figure 32. In-bore axial acceleration vs. time.

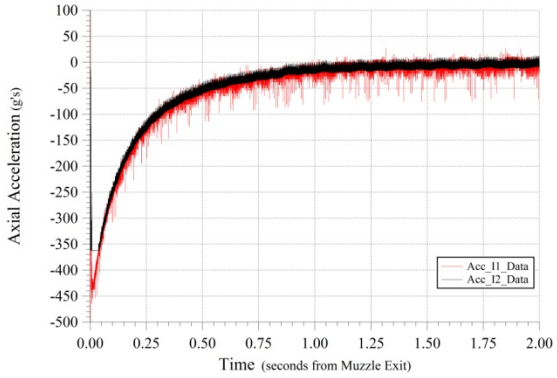

Figure 33. Axial acceleration vs. time.

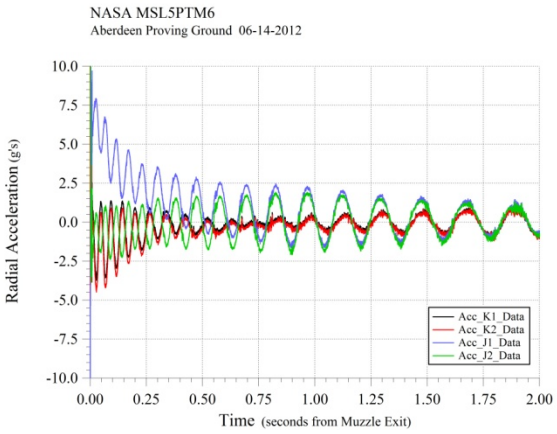

Figure 34. Radial acceleration vs. time.

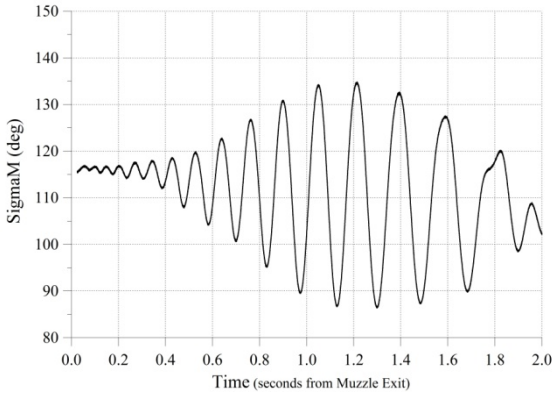

Figure 35. Magnetic aspect angle vs. time.

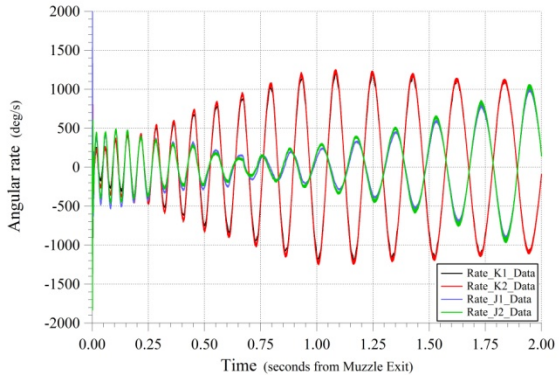

Figure 36. Pitch and yaw angular rate vs. time.

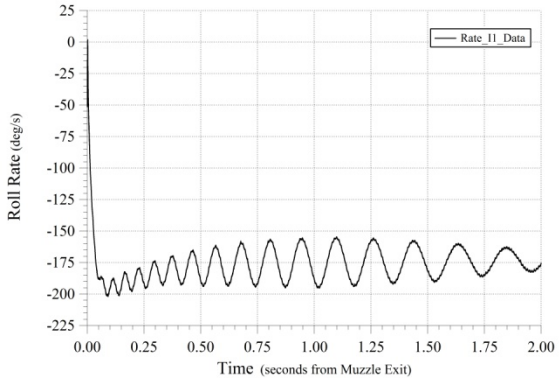

Figure 37. Roll rate vs. time.

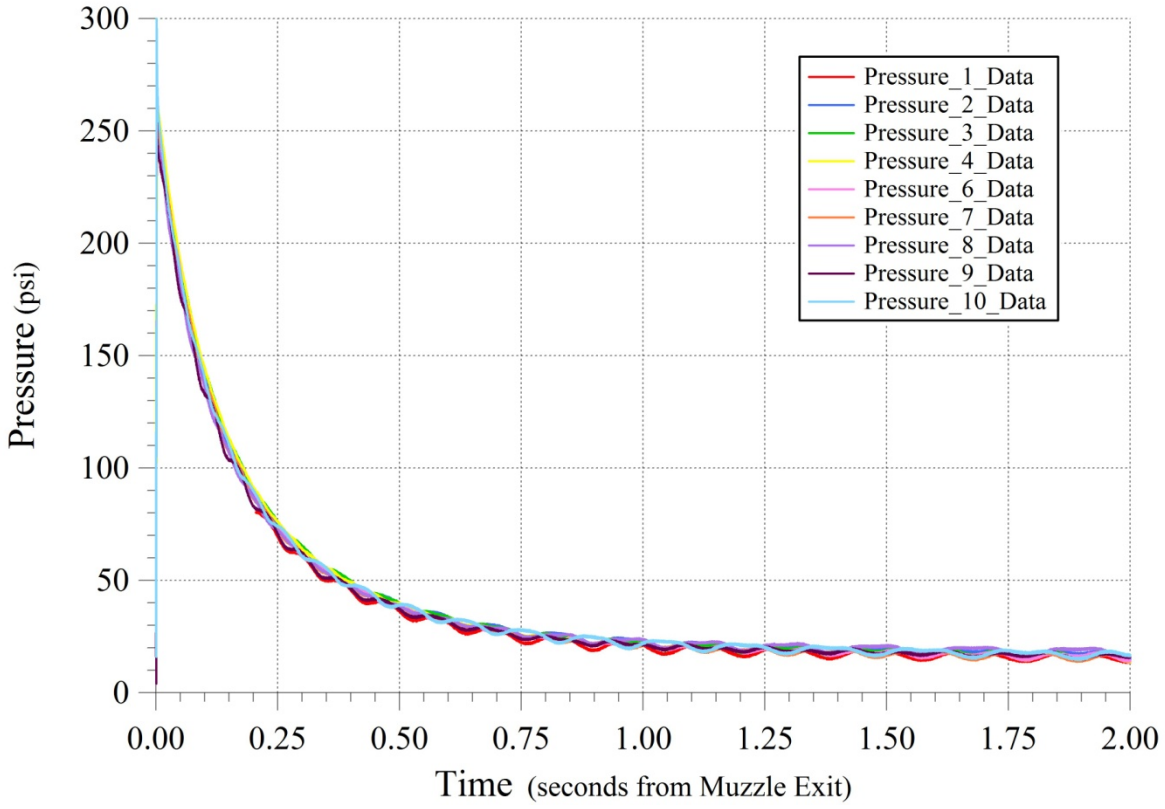

Figure 38. Pressure vs. time from MSL5PTM6.

NASA LaRC was able to use the data to reconstruct the representative trajectories and determine the proper aerodynamics parameters that match the Mach number, angle of attack, and sideslip (*9, 10*). NASA's reconstruction results from the pressure transducer data, magnetometer data, and IMU data were analyzed using two different solution methodologies that varied based on the data chosen, and included the PTM configuration locations and MSL Entry Atmospheric Data Systems (MEADS) configuration locations. The MEADS technique uses only 7 of the 10 PTM pressure transducers. NASA compared these results with a third solution that did not use the pressure data but did include the radar-derived body velocities (radar), as shown in figure 39 for MSL5PTM6. Similar results were achieved by all three with a slight bias (about 2°) for the radar solution. Lugo et al. (*9*) stated that biases in the angle of attack determinations may be attributed to error sources from the accelerometer and/or magnetometer (used in the radar solution), biases in the pressure data, and/or imperfections in the CG location. The pressure history data for the MSL-PTM lifting bodies, shown in figures 40 and 41, was provided to NASA for trajectory reconstruction as well.

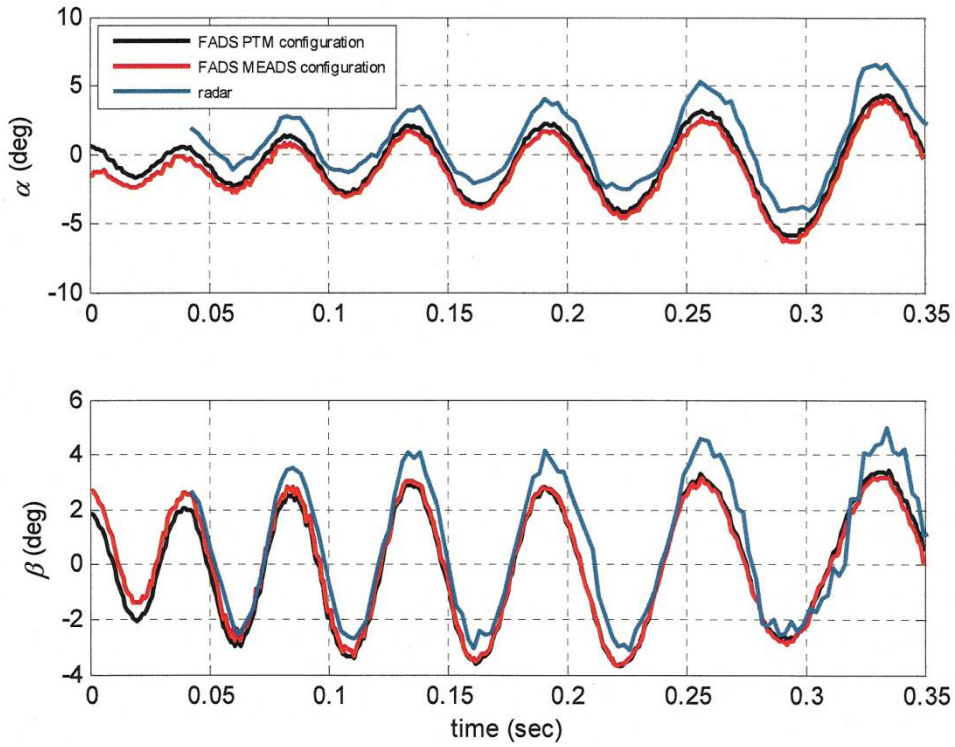

Figure 39. NASA LaRC alpha-beta reconstruction comparisons.

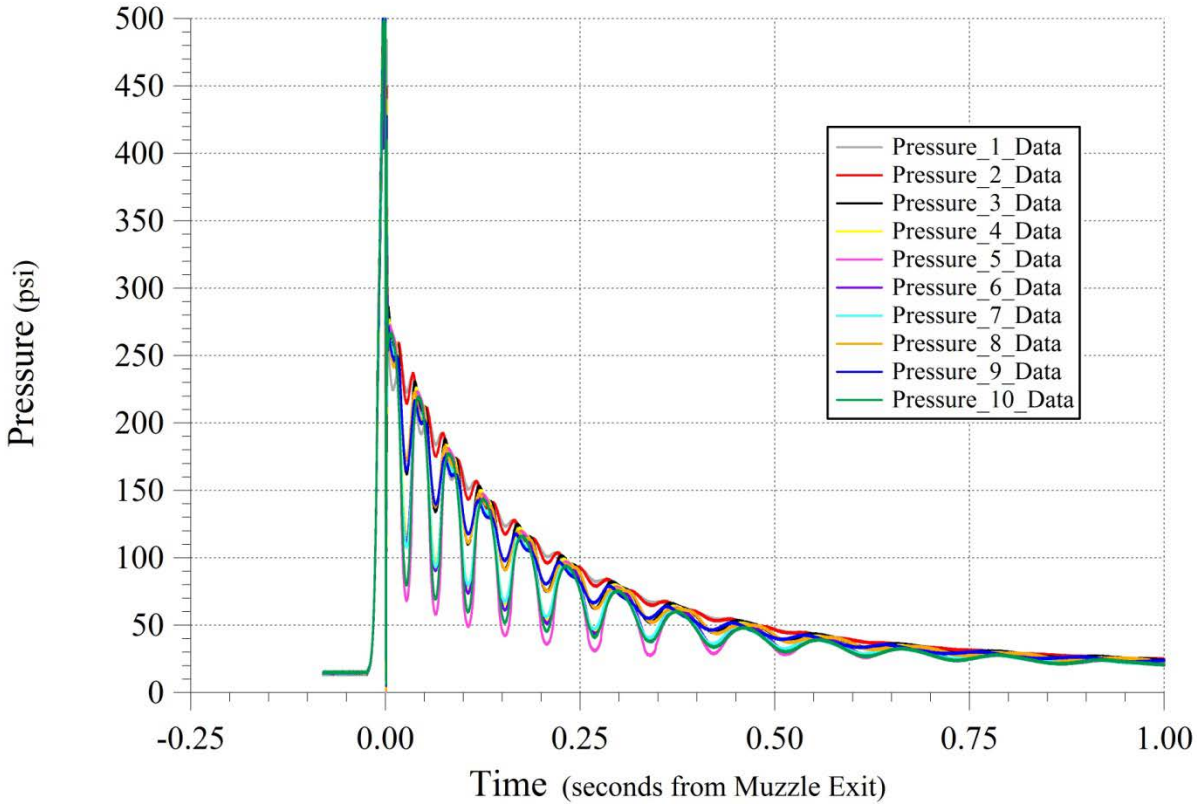

Figure 40. Pressure vs. time from MSL8PTM9.

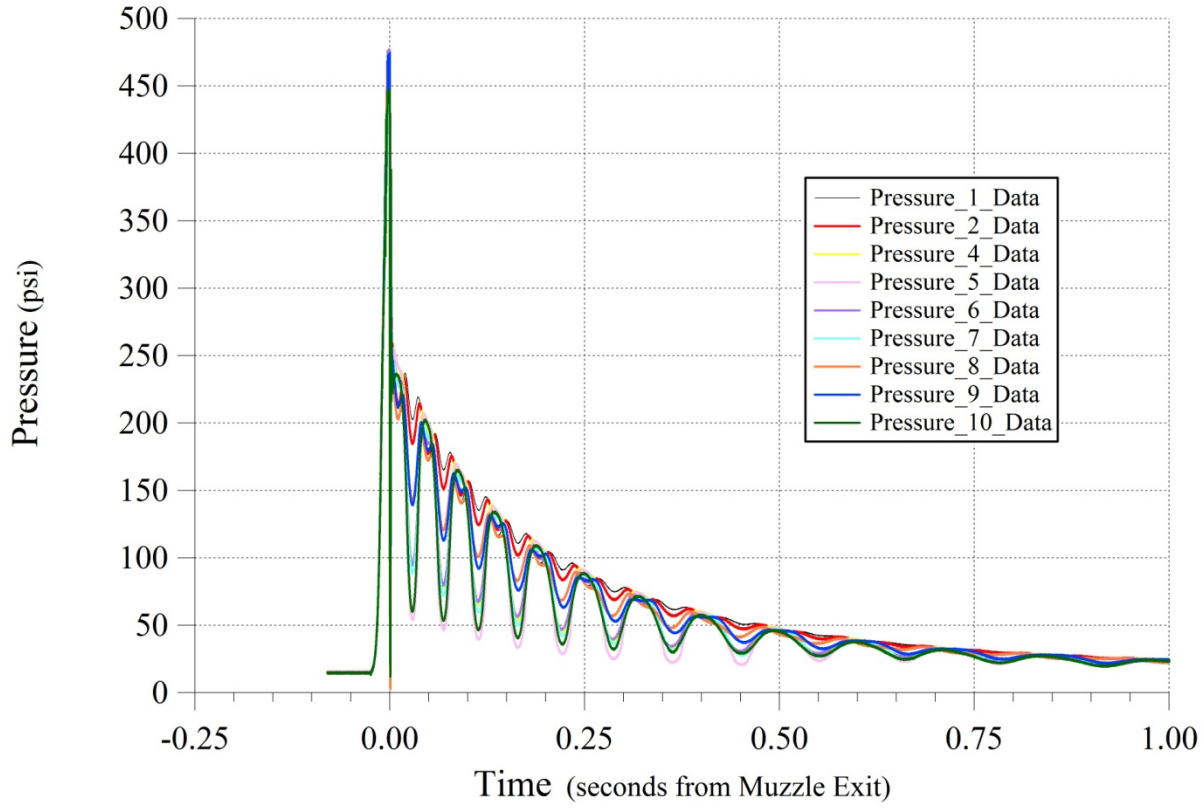

Figure 41. Pressure vs. time from MSL7PTM5.

4. Conclusion

ARL was successful in providing NASA LaRC with the instrumented hardware and experimental data necessary to reconstruct the trajectory of the MSL capsule simulating entry into the atmosphere of Mars. The novel approach involved using a large-caliber HARP gun to launch a saboted model that was a subscale replica of the actual MSL spacecraft at a velocity of nearly Mach 4. Success in this endeavor was dependent on meeting several objectives. Once launched from the gun, the flight body needed to lift vertically upward, creating a trajectory curve unlike most ballistic flight experiments. To achieve this lifting trajectory, the CG and overall weight of the models were critical. Thus high precision was required in the mechanical design process to locate the CG and meet the desired weight requirement. The experimental subscale model also required an onboard MIDAS telemetry system to send IMU and pressure sensor information to a ground receiving station while in flight. Another key component that was successfully demonstrated was a sabot that properly oriented the models and quickly separated after muzzle exit. Radar lock-on experiments of 100-mm scale models and 100-mm ballistic slugs were needed and proved beneficial, as the radar technicians learned valuable lessons about the capabilities of the tracking radar that would eventually track the 171-mm scale MSL models.

Launching the 100-mm subscale models also showed how in-bore rotation of the sabot package during launch affected the experimental results. Launching the 171-mm MSL models revealed that the angled sabots were not separating properly, and material was removed to alleviate the issue. The culmination of all these efforts provided the desired flight profile, successful radar lock, telemetry data capture, and flight dynamics data processing of the instrumented MSL-PTM flight bodies.

5. References

1. Topper, B.; Brown, T.; Bukowski, E.; Davis, B.; Hall, R.; Muller, P.; Vong, T.; Brandon, F. *Feasibility of Determining Aerodynamic Coefficients for a NASA Apollo Body With the Use of Telemetry Data From Free Flight Range Testing;* ARL-TR-4271; U.S. Army Research Laboratory: Aberdeen Proving Ground, September 2007.

2. Muller, P.; Davis, B.; Condon, J.; Topper, B. Characterizing Smart Munitions Flight Behavior with a Multifunctional Instrumentation and Data Acquisition System (MIDAS). Presented at the ITEA Test Instrumentation Workshop, Las Vegas, NV, 2010.

3. Topper, B.; Muller, P. NASA Orion Crew Exploration Vehicle – Pressure Telemetry Module Free Flight Ballistic Range Experiment. Presented at the ARL State Estimation Workshop, 2011.

4. Sebastian, T.; Tolson, R. H. Methods for the Determination of Aerodynamic Parameters and Trajectory Reconstruction of the Orion Command Module from Scale Model Aeroballistic Flight Data. Presented at the 47th AIAA Aerospace Sciences Meeting Including The New Horizons Forum and Aerospace Exposition, Orlando, FL, 2009.

5. Lugo, R. A. Methods of Flight Parameter Recovery from Orion Crew Module Using Scale Model Aeroballistic Flight Data. Master's thesis, North Carolina State University, Raleigh, NC, 2011.

6. Murphy, C. M.; Bull, G. V. *Review of the High Altitude Research Program (HARP);* BRL-TR-1327; U.S. Army Ballistics Research Laboratory: Aberdeen Proving Ground, MD, 1966.

7. Guidos, B.; Sorensen, B.; Phillabaum, R. HARP Guns: Status and Recent Firings. Presented at the 60th Meeting of the Aeroballistic Range Association, Baltimore, MD, 2009.

8. Guidos, B. J. Innovative Design and Use of Cylindrical Ballistic Slugs in Gun Firings. Presented at the 62nd Annual Meeting of the Aeroballistic Range Association, Put-in-Bay, OH, 2011.

9. Lugo, R. A.; Tolson, R. H.; Schoenenberger, M .Trajectory Reconstruction and Uncertainty Analysis Using Mars Science Laboratory Pre-Flight Scale Model Aeroballistic Testing. Presented at 51st American Institute of Aeronautics and Astronautics Aerospace Sciences Meeting, Grapevine, TX, January 2013.

INTENTIONALLY LEFT BLANK.

Appendix. Mars Science Lab Pressure Transducer Module Pressure Calibration Results

This appendix appears in its original form, without editorial change.

	MSL5PTM6		MSL6PTM7		MSL7PTM5		MSL8PTM9	
Port	Bias (psi)	Scale Factor (psi/bit)	Bias (psi)	Scale Factor (psi/bit)	Bias (psi)	Scale Factor (psi/bit)	Bias (psi)	Scale Factor (psi/bit)
1	-119.50	0.1544	-106.14	0.1531	-151.46	0.1500	-112.41	0.1540
2	-102.04	0.1549	-115.83	0.1538	-150.65	0.1510	-134.54	0.1532
3	-129.04	0.1551	-121.10	0.1526	34143.00	-8.4437	-129.09	0.1535
4	-118.70	0.1546	-121.25	0.1529	-150.08	0.1515	-115.06	0.1522
5	-6973.00	8.2281	-120.16	0.1531	-148.85	0.1493	-118.89	0.1536
6	-121.22	0.1549	-516.64	0.5497	-134.71	0.1511	-124.13	0.1543
7	-114.27	0.1549	-111.01	0.1533	-149.76	0.1514	-119.10	0.1534
8	-106.09	0.1549	-120.29	0.1523	-144.23	0.1504	-119.86	0.1524
9	-124.70	0.1551	-2686.70	334.4100	-139.12	0.1509	-105.75	0.1539
10	-119.62	0.1549	-120.88	0.1534	-158.16	0.1491	-119.68	0.1536

Those in red denote transducer that were not working properly

	MSL5PTM6		MSL6PTM7		MSL7PTM5		MSL8PTM9	
Port	Bias (kPa)	Scale Factor (kPa/bit)	Bias (kPa)	Scale Factor (kPa/bit)	Bias (kPa)	Scale Factor (kPa/bit)	Bias (kPa)	Scale Factor (kPa/bit)
1	-823.92	1.064	-731.81	1.055	-1044.28	1.034	-775.04	1.061
2	-703.54	1.068	-798.62	1.060	-1038.70	1.041	-927.62	1.056
3	-889.70	1.070	-834.96	1.052	235407.70	-58.217	-890.04	1.058
4	-818.41	1.066	-835.99	1.054	-1034.77	1.044	-793.31	1.049
5	-48077.14	56.731	-828.47	1.055	-1026.28	1.030	-819.72	1.059
6	-835.78	1.068	-3562.11	3.790	-928.79	1.042	-855.85	1.064
7	-787.86	1.068	-765.39	1.057	-1032.56	1.044	-821.17	1.057
8	-731.46	1.068	-829.37	1.050	-994.43	1.037	-826.41	1.051
9	-859.78	1.069	-18524.14	2305.676	-959.20	1.040	-729.12	1.061
10	-824.75	1.068	-833.44	1.057	-1090.47	1.028	-825.16	1.059

Those in red denote transducers that were not working properly

NO. OF COPIES	ORGANIZATION
1 (PDF)	DEFENSE TECHNICAL INFORMATION CTR DTIC OCA
1 (PDF)	DIRECTOR US ARMY RESEARCH LAB IMAL HRA
1 (PDF)	DIRECTOR US ARMY RESEARCH LAB RDRL CIO LL
1 (PDF)	GOVT PRINTG OFC A MALHOTRA
1 (PDF)	RDRL WML F D PETRICK

INTENTIONALLY LEFT BLANK.